ACCOUNTS of chemical research

Article

pubs.acs.org/accounts

Insight into the Structure and Mechanism of Nickel-Containing Superoxide Dismutase Derived from Peptide-Based Mimics

Jason Shearer

Department of Chemistry, University of Nevada, Reno, Reno, Nevada 89557, United States

Supporting Information

CONSPECTUS: Nickel superoxide dismutase (NiSOD) is a nickel-containing metalloenzyme that catalyzes the disproportionation of superoxide through a ping-pong mechanism that relies on accessing reduced Ni(II) and oxidized Ni(III) oxidation states. NiSOD is the most recently discovered SOD. Unlike the other known SODs (MnSOD, FeSOD, and (CuZn)SOD), which utilize "typical" biological nitrogen and oxygen donors, NiSOD utilizes a rather unexpected ligand set. In the reduced Ni(II) oxidation state, NiSOD utilizes nitrogen ligands derived from the N-terminal amine and an amidate along with two cysteinates sulfur donors. These are unusual biological ligands, especially for an SOD: amine and amidate donors are underrepresented as biological ligands, whereas cysteinates are highly susceptible to oxidative damage. An axial histidine imidazole binds to nickel upon oxidation to Ni(III). This bond is long (2.3−2.6 Å) owing to a tight hydrogen-bonding network.

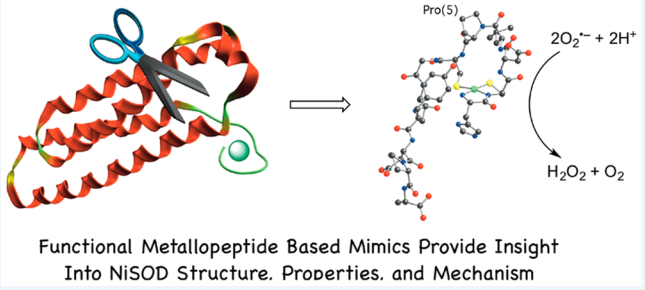

Functional Metallopeptide Based Mimics Provide Insight Into NiSOD Structure, Properties, and Mechanism

All of the ligating residues to Ni(II) and Ni(III) are found within the first 6 residues from the NiSOD N-terminus. Thus, small nickel-containing metallopeptides derived from the first 6−12 residues of the NiSOD sequence can reproduce many of the properties of NiSOD itself. Using these nickel-containing metallopeptide-based NiSOD mimics, we have shown that the minimal sequence needed for nickel binding and reproduction of the structural, spectroscopic, and functional properties of NiSOD is H_2N-HCXXPC.

Insight into how NiSOD avoids oxidative damage has also been gained. Using small NiN_2S_2 complexes and metallopeptide-based mimics, it was shown that the unusual nitrogen donor atoms protect the cysteinates from oxidative damage (both one-electron oxidation and oxygen atom insertion reactions) by fine-tuning the electronic structure of the nickel center. Changing the nitrogen donor set to a bis-amidate or bis-amine nitrogen donor led to catalytically nonviable species owing to nickel−cysteinate bond oxidative damage. Only the amine/amidate nitrogen donor atoms within the NiSOD ligand set produce a catalytically viable species.

These metallopeptide-based mimics have also hinted at the detailed mechanism of SOD catalysis by NiSOD. One such aspect is that the axial imidazole likely remains ligated to the Ni center under rapid catalytic conditions (i.e., high superoxide loads). This reduces the degree of structural rearrangement about the nickel center, leading to higher catalytic rates. Metallopeptide-based mimics have also shown that, although an axial ligand to Ni(III) is required for catalysis, the rates are highest when this is a weak interaction, suggesting a reason for the long axial His−Ni(III) bond found in NiSOD. These mimics have also suggested a surprising mechanistic insight: O_2^- reduction via a "$H^{\bullet}$" tunneling event from a R−S(H^+)−Ni(II) moiety to O_2^- is possible. The importance of this mechanism in NiSOD has not been verified.

INTRODUCTION

Superoxide (O_2^-), a reactive oxygen species (ROS) that is formed from the one-electron reduction of O_2, and is the precursor for a number of other highly toxic ROSs, including H_2O_2, $HO^{\bullet}$, ONO_2^-, and ClO^-.[1−4] Many organisms have developed enzymes that degrade O_2^- before it can facilitate cellular damage, of which superoxide dismutases (SODs) are the most prevalent O_2^- detoxification enzymes.[5−7] All known SODs contain a redox-active metal cofactor and catalyze the disproportionation of O_2^- by accessing oxidized and reduced oxidation states through a highly efficient ping-pong mechanism ($k_{cat} \sim 10^9$ M^{-1} s^{-1}).[5−8]

$$O_2^- + 2H^+ + SOD^{red} \rightarrow H_2O_2 + SOD^{ox} \quad (1a)$$

$$SOD^{ox} + O_2^- \rightarrow SOD^{red} + O_2 \quad (1b)$$

There are four known classes of SODs: (Cu/Zn)SOD, MnSOD, FeSOD, and NiSOD (Chart 1 and Scheme 1). (Cu/Zn)SOD, MnSOD, and FeSOD have been extensively studied and contain metal cofactors in N/O coordination spheres.[5,8] Less thoroughly studied is NiSOD, which possesses a cysteinate-rich active site.[6,7] Cysteinate ligands were

Received: February 10, 2014
Published: May 13, 2014

   dx.doi.org/10.1021/ar500060s | Acc. Chem. Res. 2014, 47, 2332−2341

Chart 1. Active-Site Structures of Cu/Zn-, Mn-, and FeSOD

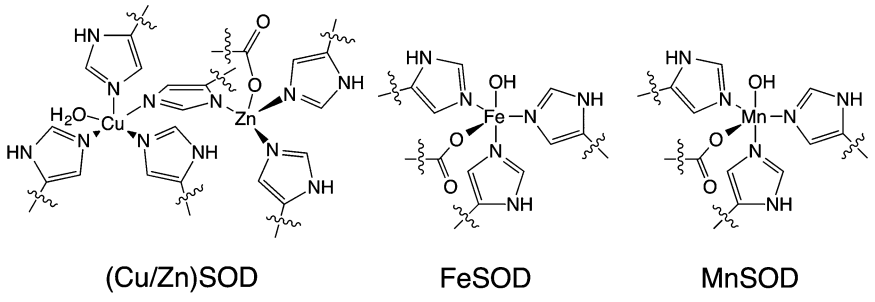

Scheme 1. Active-Site Structure and Reaction Performed by NiSOD

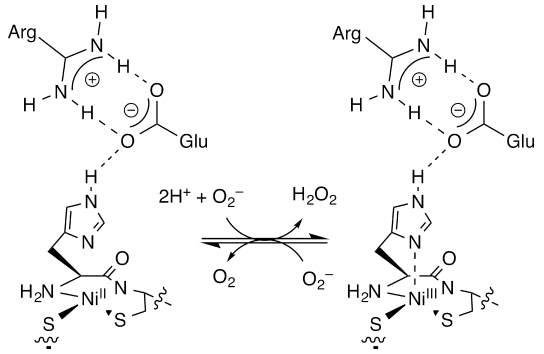

unexpected because the thiolate–Ni bond is susceptible to oxidative damage.[9] Understanding how the Ni–S^{Cys} bond at the NiSOD active site avoids oxidative damage, along with other aspects of NiSOD chemistry, is a current focus of research in my group. Because there are several excellent reviews focused on NiSOD,[6,7,10] only the key points concerning NiSOD relevant to this Account will be discussed.

Originally isolated form *Streptomyces* species in 1996, NiSOD was later found to be widely represented in aquatic microbes.[11−14] Initial spectroscopic studies demonstrated that NiSOD contains cysteinate ligands along with other nitrogen-based donors bound to nickel in both reduced (Ni^{II}) and oxidized (Ni^{III}) oxidation states.[10−12,15−17] This supposition was confirmed by X-ray crystallography.[18−20]

Active NiSOD is homohexameric, with each subunit containing a catalytically active nickel ion. Pertinent to this work is the fact that all of the ligating residues to Ni are contained within the first six residues from the NiSOD N-terminus (termed the Ni-binding hook). In the apoprotein, this hook is disordered, adopting a well-defined structure only upon nickel coordination.[18,19] In the Ni(II) oxidation state, the nickel ion is ligated in a square planar N_2S_2 coordination geometry with ligands derived from the N-terminal amine, an amidate from Cys(2), and cysteinate ligands from Cys(2) and Cys(6) (Scheme 1). Upon oxidation to Ni(III), the His(1) imidazole coordinates to nickel, forming a square pyramidal structure. The axial His(1) imidazole–Ni(III) bond is longer than expected (~2.2–2.6 Å long). This is likely the result of a tight hydrogen-bonding network among it, a glutamate, and an arginine residue that "locks" the imidazole in place.[18,19,21,22]

The NiSOD active site possesses a number of unusual structural features. First, the nitrogen donors in the equatorial plane are underrepresented in nature: ligation of nitrogen atoms derived from amidates or the protein N-terminal amine are observed only in a handfull of metalloenzymes.[6,7,23−25] More unusual are the cysteinate ligands. All known redox-active nickel enzymes possess cysteinate or redox noninnocent ligands.[26] Therefore, the cysteinates likely tune the Ni(II)/Ni(III) redox couple such that it is within the range of the superoxide reduction (−0.16 V vs NHE) and oxidation (+0.89 V vs NHE) couples.[4] However, metal-cysteinates are highly susceptible to oxidative damage, making them seemingly unsuitable for SOD chemistry.[9]

To better understand the structure and other aspects of NiSOD chemistry, we[14,27−35] and others (see the review by Harrop[6]) have prepared a number of small synthetic models of the NiSOD active site. This Account will focus on our work involving metallopeptide-based mimics of NiSOD derived from the NiSOD primary sequence (Dutton's metalloprotein maquette approach).[36] In the metalloprotein maquette approach, one prepares small metallopeptides that contain key protein sequences found in the parent metalloprotein. This approach thus allows one to tease out key structural and sequence-dependent features of a protein that contribute to its properties and function.[36,37] We have found that this approach is well-suited for understanding the properties of NiSOD.

MINIMAL STRUCTURAL REQUIREMENTS FOR NICKEL COORDINATION AND CATALYSIS WITHIN NISOD

As all of the Ni-coordinating ligands are contained within the first six residues from the N-terminus of the NiSOD sequence, a nickel-containing metallopeptide derived from the first 12 residues of the *Streptomyces coelicolor* NiSOD sequence was prepared ({Ni(SOD^{m1})}; SOD^{m1} = HCDLPCGVYDPA).[28] {Ni^{II}(SOD^{m1})} possesses a UV–vis spectrum reminiscent of reduced NiSOD at physiological pH (Figure 1). The initially reported CD spectrum of as isolated {Ni^{II}(SOD^{m1})} contained contributions from {Ni^{III}(SOD^{m1})} produced from the oxidation of {Ni^{II}(SOD^{m1})} by trace O_2. Following ascorbate reduction, {Ni^{II}(SOD^{m1})} yields a CD spectrum that is nearly identical to reduced NiSOD. Ni K-edge XAS demonstrated {Ni^{II}(SOD^{m1})} possesses a square planar $Ni^{II}N_2S_2$ center with metric parameters similar to reduced NiSOD (Figure 2 and Table S1, Supporting Information). These data show that both the Ni(II) and Ni(III) oxidation states can be stabilized by SOD^{m1} and that and the Ni(II) center of {Ni^{II}(SOD^{m1})} is structurally similar to the NiSOD active site.

Further studies revealed that {Ni(SOD^{m1})} is SOD-active. Thin-film metallopeptide cyclic voltammetry (CV) showed that {Ni(SOD^{m1})} has a quasi-reversible Ni^{II}/Ni^{III} couple at 0.71 V versus NHE,[28] whereas solution measurements place the redox couple at 0.639 V vs NHE.[31] This demonstrates that the redox couple for {Ni(SOD^{m1})} is between the O_2^- oxidation and reduction couples, which shows that {Ni^{II}(SOD^{m1})} is

dx.doi.org/10.1021/ar500060s | Acc. Chem. Res. 2014, 47, 2332−2341

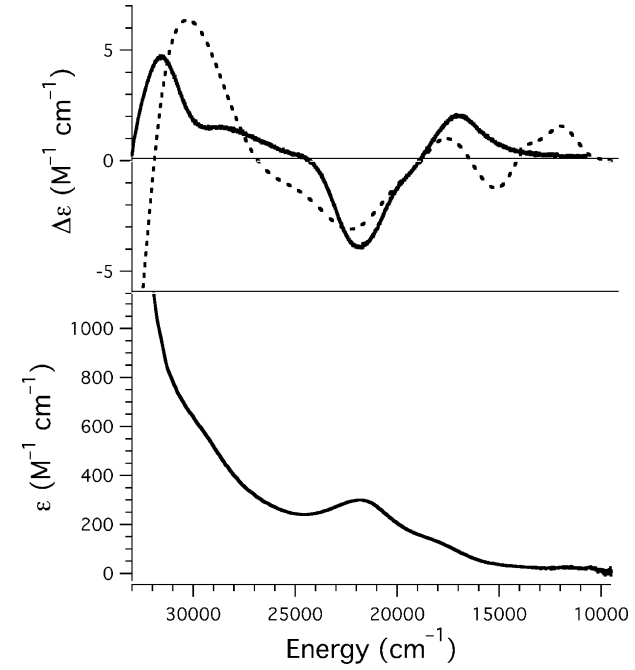

Figure 1. (A) Electronic absorption and (B) CD spectrum of reduced (solid line) and partially oxidized (dashed line) {Ni^{II}(SOD^{m1})}.

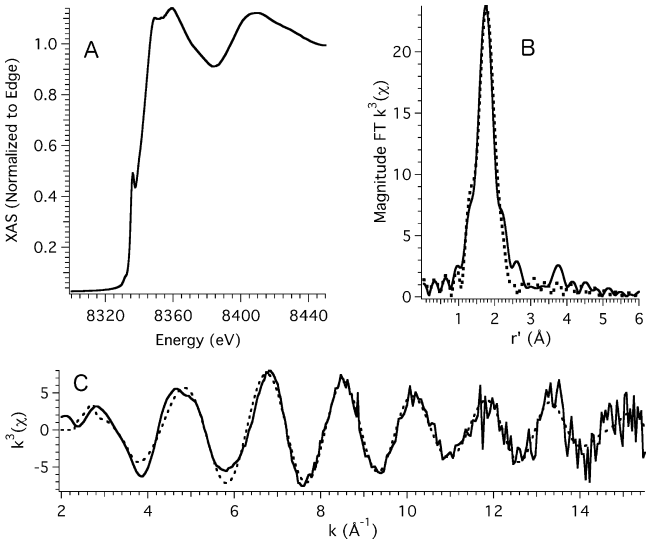

Figure 2. Ni K-edge X-ray absorption spectrum of {Ni^{II}(SOD^{m1})} displaying the edge portion of the spectrum (A), the k^3-weighted EXAFS (B), and FT k^3-weighted EXAFS (C). The data are the solid spectra, and the simulations are the dashed spectra.

electrochemically poised for SOD activity. Stopped-flow kinetic studies demonstrated that {Ni(SOD^{m1})} is, in fact, a competent SOD (k_{cat} = 4(3) × 10^7 M^{-1} s^{-1} vs 7 × 10^8 M^{-1} s^{-1} for *S. coelicolor* NiSOD). Thus, the Ni-binding hook in and of itself can generate a functional SOD-active nickel peptide that is structurally similar to NiSOD. Following our work, other researchers have reached similar conclusions.[6,38,39]

Derivatives of {Ni(SOD^{m1})} were prepared to determine the minimum structural features required for Ni binding and SOD activity (Chart 2). {Ni^{II}(SOD^{m2})} (SOD^{m2} = HCDLPCG) possesses similar structural, spectroscopic, and reactive properties as those of {Ni(SOD^{m1})}, suggesting residues outside the loop region of the Ni-binding hook have minimal influence on

Chart 2. Metal Center Structures of {Ni^{II}(SOD^{m2})} Derivatives

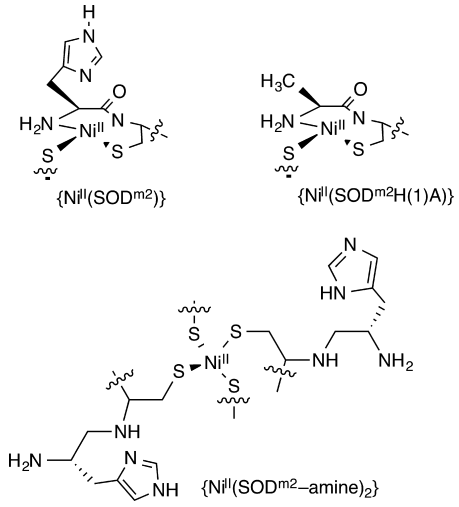

nickel binding and SOD activity.[30] The largest difference between {Ni^{II}(SOD^{m2})} and {Ni^{II}(SOD^{m1})} is a +80 mV shift in redox potential, which may be attributable to a higher solvent accessibility of the Ni center upon removal of the noncoordinating peptide tail. The His(1)Ala derivative of {Ni^{II}(SOD^{m2})} ({Ni^{II}(SOD^{m2}H(1)A)}) yields a metallopeptide that will coordinate Ni(II) in a manner identical to {Ni^{II}(SOD^{m2})} but is SOD-inactive. Altering the Cys(2) amidate to an amine nitrogen results in a tetrahedral NiS$_4$ center with cysteinates derived from two peptides ({Ni(SOD^{m2}-amine)$_2$}; Table S1, Supporting Information and Figure 3).[40]

In a combined bioinformatics/modeling collaborative study with DuPont and Palenik, we examined the influence of noncoordinating residues within the nickel-binding hook.[14] Sequence alignments suggest that His(1), Cys(2), Pro(5), and Cys(6) are conserved in NiSOD-like proteins. By systematically

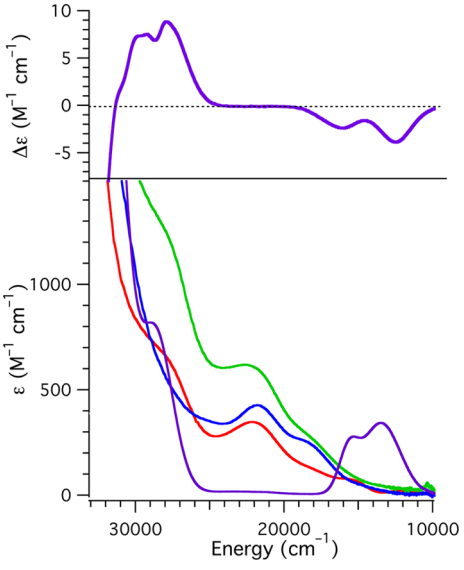

Figure 3. Bottom: Electronic absorption spectra of {Ni^{II}(SOD^{m2})} (blue), {Ni^{II}(SOD^{m2}-H(1)A)} (red), {Ni^{II}(SOD^{m1}-Ac)} (green), and {Ni^{II}(SOD^{m2}-amine)$_2$} (purple). Top: CD spectrum of {Ni^{II}(SOD^{m2}-amine)$_2$}.

dx.doi.org/10.1021/ar500060s | *Acc. Chem. Res.* 2014, 47, 2332−2341

Chart 3. Structures of Model Compounds Used To Probe the Influence of Amine/Amidate Ligation on $Ni^{II}N_2S_2$ Complexes

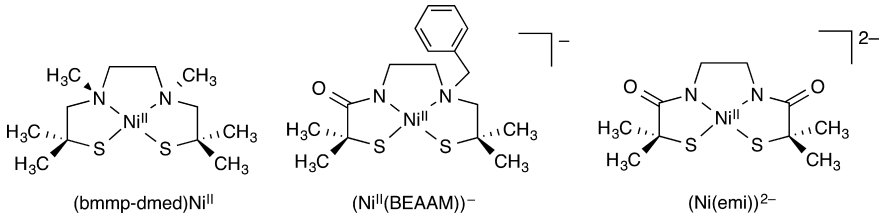

altering the noncoordinating residues within the Ni-binding hook of $\{Ni^{II}(SOD^{m1})\}$ to alanine, we unambiguously demonstrated that the only vital noncoordinating residue within the Ni-binding hook that is required for Ni binding and subsequent SOD activity is Pro(5). We propose that Pro(5) enforces a turn-like structure within the Ni-binding hook, providing an entropic driving force for $Ni-S^{Cys(6)}$ coordination. These results all suggest that H_2N-HCXXPC is the minimal peptide motif required for Ni binding and SOD activity within a NiSOD-like coordination motif.

CYSTEINATE STABILITY AND THE MIXED AMINE/AMIDATE LIGAND SET

To better understand the influence of the amine/amidate ligand set on the NiSOD nickel center, we initially examined the properties of three $Ni^{II}N_2S_2$ complexes (Chart 3): amine/amidate-ligated $(Ni^{II}(BEAAM))^-$,[33,34] bis-amine-ligated (bmmp-dmed)Ni^{II},[41] and bis-amidate-ligated $(Ni^{II}(emi))^{2-}$.[42] Because this represents a slight digression from our research regarding metallopeptide-based mimics, only the key findings from these small molecule studies will be provided below.

Our spectroscopic and computational studies strongly suggested that the amine and amidate ligands play a key role in protecting the Ni-cysteinates from oxidative damage.[34] The HOMO for all three complexes is derived from a highly covalent Ni(3dπ)/S(3pπ*) antibonding interaction (Scheme 2). As the neutral amine ligands are systematically replaced with anionic amidate ligands, the whole 3d set is destabilized. This results in a better energy match between the Ni(3dπ) orbitals and the high-lying S(3pπ*) molecular orbital fragments. The consequence of this is that the degree of S character comprising the HOMO decreases concomitant with HOMO activation. The reduction in S character to the HOMO will lead to a more Ni-centered oxidation process, which will better stabilize the Ni(III) oxidation state owing to a reduction in S radical character to the SOMO. This, in turn, protects the thiolate ligands from one-electron oxidative damage upon redox cycling, as evidenced by CV studies. Bis-amine-ligated (bmmp-dmed)-Ni^{II} shows an irreversible oxidation wave,[41] whereas both $(Ni^{II}(BEAAM))^-$ and $(Ni(emi))^{2-}$ display reversible Ni^{II}/Ni^{III} redox processes.[33,42] Conversely, HOMO activation will render the Ni-thiolates more susceptible to oxidative electrophilic attack by O_2 and H_2O_2. This is revealed by exposing acetonitrile solutions of the complexes to O_2: both (bmmp-dmed)Ni^{II} and $(Ni^{II}(BEAAM))^-$ are O_2 stable, whereas bis-amidate-ligated $(Ni(emi))^{2-}$ rapidly undergoes Ni-sulfinate formation. These results suggest that the mixed amine/amidate ligand set is electronically fine-tuning the NiSOD active site to protect the cysteinates from oxidative damage.

Scheme 2. Ni and S Molecular Orbital Fragment Overlap and Resulting HOMO for (bmmp-dmed)Ni^{II}, $(Ni^{II}(BEAAM))^-$, and $(Ni^{II}(emi))^{2-}$

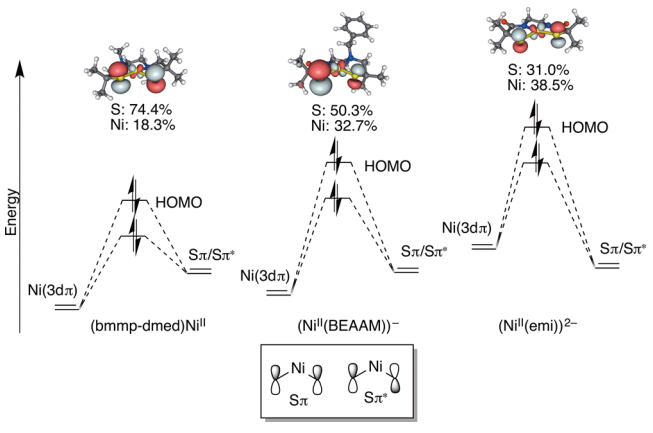

Prior to the publication of the experimental work summarized above, Grapperhaus and co-workers published a computational study that reached similar conclusions regarding the protective ability of the mixed amine/amidate ligand set on the $Ni-S^{Cys}$ bond.[43] Also, a recent study by Grapperhaus examining H_2O_2 induced thiolate oxidation of an amine/amide-ligated N_3S Ni(II) complex lends further evidence for the slow rate of oxidation of such compounds.[44] On the basis of that study, we can estimate a reaction half-life for $\{Ni(SOD^{m1})\}$ oxidation by H_2O_2 under our catalytic conditions (pH 8.0, 50 mM KO_2, 1 mM $\{Ni(SOD^{m1})\}$) of ~29 s following the disproportionation reaction. These conditions represent lethal levels of H_2O_2. As Grapperhaus has pointed out, under high sublethal H_2O_2 concentrations, NiSOD itself should have a half-life of ~117 min. This demonstrates that cellular NiSOD is quite stable against such oxidation events even when product dissociation from the active site and subsequent H_2O_2 detoxification are not considered.

The supposition that the mixed amine/amidate ligand set is protecting the cysteinate sulfur atoms from oxidative damage was further probed by comparing $\{Ni(SOD^{m1})\}$ with bis-amidate-ligated $\{Ni(SOD^{m1}\text{-Ac})\}$ (Scheme 3 and Table S1, Supporting Information).[29,32] Spectroscopically and structurally, the two metallopeptides are similar, displaying the expected systematic changes in spectroscopic signatures, electronic structures, and structural properties expected for the amine/amidate to bis-amidate modification.[29,33−35] Of note is the −120 mV shift in the Ni^{II}/Ni^{III} redox potential of $\{Ni^{II}(SOD^{m1}\text{-Ac})\}$ (519 mV vs NHE) relative to $\{Ni^{II}(SOD^{m1})\}$. $\{Ni^{II}(SOD^{m1}\text{-Ac})\}$ should therefore be the better SOD, as its Ni^{II}/Ni^{III} couple is closer to the average of the O_2^- oxidation and reduction couples. However, $\{Ni^{II}(SOD^{m1}\text{-Ac})\}$ is catalytically inactive.[32] This is because a coordinated cysteinate is being oxidized upon exposure of $\{Ni^{II}(SOD^{m1}\text{–Ac})\}$ to O_2^- (and O_2).

IR studies and S K-edge X-ray absorption spectroscopy show the complete conversion of solutions of $\{Ni^{II}(SOD^{m1}\text{-Ac})\}$ to

dx.doi.org/10.1021/ar500060s | Acc. Chem. Res. 2014, 47, 2332−2341

Scheme 3. Effect of O_2 Exposure to Amine/Amidate-Ligated $\{Ni^{II}(SOD^{m1})\}$ and Bis-Amidate-Ligated $\{Ni^{II}(SOD^{m1})\text{-Ac}\}$

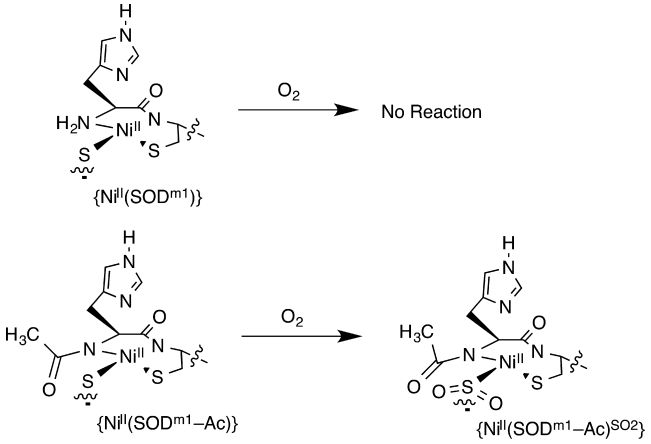

sulfinate-ligated $\{Ni^{II}(SOD^{m1}\text{-Ac})^{SO_2}\}$ under air. No sulfur-based oxidation is observed for $\{Ni^{II}(SOD^{m1})\}$ under identical conditions. Most relevant are the ESI-MS data for $\{Ni^{II}(SOD^{m1})\}$ versus $\{Ni^{II}(SOD^{m1}\text{-Ac})\}$ following KO_2 exposure. The ESI-MS of $\{Ni^{II}(SOD^{m1}\text{-Ac})\}$ following KO_2 addition shows extensive metallopeptide damage and oxidation (Figure 4), whereas the ESI-MS of $\{Ni^{II}(SOD^{m1})\}$ following KO_2 addition displays only the peak for unaltered $\{Ni^{II}(SOD^{m1})\}$. These results lend further evidence that the amine/amidate ligand set is protecting the $Ni-S^{Cys}$ bonds in NiSOD from oxidative damage.

Small molecule biomimetic studies have suggested additional factors that may contribute to the stability of the NiSOD active site. Grapperhaus and Darensbourg have suggested that oxidative damage is avoided because of the short resident time of oxidizing molecules at the NiSOD active site coupled with the slow rate of predicted cysteinate oxidation.[44,45] Harrop has suggested that $Ni-S^{Cys}\cdots H-N^{amide}$ hydrogen bonds also contribute to cysteinate stability, as small molecule $Ni^{II}N_2S_2$ complexes with $Ni-S^{R}\cdots H-N^{amide}$ hydrogen bonds undergoes slower thiolate oxidation events relative to a complex lacking such hydrogen bonding interactions.[46] We note that $\{Ni(SOD^{m1})\}$ lacks the restrained outersphere hydrogen-bonding interactions examined by Harrop. Furthermore, the nickel center of $\{Ni(SOD^{m1})\}$ is solution-exposed and is thus "bathed" in O_2, O_2^-, and H_2O_2, which will partially eliminate the influence of the short residence time of ROSs at the NiSOD active site. On the basis of these data and those presented by others (Grapperhaus in particular),[43−45] it appears that the mixed amine/amidate coordination environment is a key factor in protecting the NiSOD active site from oxidative damage.

INFLUENCE OF VARIABLE HIS(1) IMIDAZOLE LIGATION ON NISOD REACTIVITY

Owing to a strong His(1) imidazole···Glu···Arg hydrogen-bonding network at the NiSOD active site, the axial Ni(III)−N^{Im} bond is elongated in NiSOD.[22] Incorporation of intricate hydrogen-bonding interactions into small designed metallopeptides in a rational manner is extremely difficult. However, the alteration of the electronic properties of the His(1) imidazole to approximate the electronic influence of the imidazole···Glu···Arg hydrogen-bonding network is relatively straightforward.

It was reasoned that the covalent attachment of electron-withdrawing groups to the ε-nitrogen of the His(1) imidazole, making for a less Lewis-basic ligand, would electronically mimic the influence of the elongated Ni(III)−imidazole bond.[31] We therefore attached electron-withdrawing tosyl ($\{Ni(SOD^{m1}\text{-tos})\}$) or 2,4-dinitrophenyl ($\{Ni(SOD^{m1}\text{-DNP})\}$) groups to the imidazole ε-nitrogen (Chart 4). Doing so resulted in a weaker Ni(III)−imidzaole interaction relative to that of $\{Ni^{III}(SOD^{m1})\}$, as evidenced by EPR (smaller A_{zz} values relative those of to $\{Ni^{III}(SOD^{m1})\}$) and resonance Raman spectroscopy (increase in the energy of the Ni(III)−S vibrational modes relative to those of $\{Ni^{III}(SOD^{m1})\}$; Figure 5) coupled with electronic structure calculations (reduction in the Ni(III)−N^{im} force constants relative to those of $\{Ni^{III}(SOD^{m1})\}$; Table S2, Supporting Information). For comparison, the $\{Ni^{II}(SOD^{m1})\}$ derivative possessing the more electron-donating methyl group attached to the imidazole ε-nitrogen ($\{Ni^{III}(SOD^{m1}\text{-Me})\}$) produced a stronger axial imidazole Ni(III) interaction than that found in $\{Ni^{III}(SOD^{m1})\}$ (Figure 5 and Table S2, Supporting Information).

Changes to the axial donor strength were reflected in the rates of SOD catalysis: the weaker the axial imidazole interaction, the faster the rate of catalysis. We observed a 2 orders of magnitude increase in the rates of SOD catalysis across the series (k_{cat} ranged from $6(1) \times 10^6$ M^{-1} s^{-1} for $\{Ni(SOD^{m1}\text{-Me})\}$ to $6(2) \times 10^8$ M^{-1} s^{-1} for $\{Ni(SOD^{m1}\text{-tos})\}$). NiSOD, which has a weaker axial Ni−imidazole interaction and more covalent Ni−S bonds than any of the maquettes investigated, displays the highest catalytic rates ($k_{cat} \sim 1 \times 10^9$ M^{-1} s^{-1}). It therefore appears that a weak Ni(III)−N^{Im} interaction is required for optimal SOD catalysis.

The reason for the change in catalytic rates was initially attributed to a reduction in the energy barrier for structural rearrangement about the Ni center during redox cycling resulting from the weaker axial Ni(III)−N bond. Another possible explanation may involve the finer details of the NiSOD mechanism. Experimental evidence points toward an outer-sphere mechanism for SOD catalysis.[19,22,30] Thus, there must be an efficient ET pathway from the O_2^- molecule to the Ni center. A highly covalent Ni−S bond could be involved in the ET pathway, as in blue copper proteins.[47] The maquettes with the weaker axial Ni(III)−imidazole interaction have more covalent Ni−S bonds that may enhance SOD catalysis because of a more efficient ET pathway.

MECHANISTIC INSIGHT DERIVED FROM NISOD MAQUETTES

NiSOD operates near the diffusion limit and must, therefore, undergo rapid redox chemistry. This would preclude a large barrier to structural rearrangement about the active site during catalysis. To gain insight into the degree of structural rearrangement about the Ni center during catalysis, two NiSOD maquettes, $\{Ni(SOD^{m2})\}$ and $\{Ni(SOD^{m2}H(1)A)\}$, were subjected variable-scan-rate thin-film CV studies.[30]

At slow scan velocities (10 mV/s), $\{Ni(SOD^{m2}H(1)A)\}$, which lacks a tethered axial ligand, displayed a reversible Ni^{II}/Ni^{III} redox process with an $E_{1/2}$ = 866 mV versus NHE and a narrow peak-to-peak separation. Increasing the scan velocity yielded "trumpeting" behavior characteristic of a reversible redox process.[48] $\{Ni(SOD^{m2})\}$, in contrast, showed a large peak-to-peak separation at slow scan velocities, which narrowed considerably at fast scan velocities, eventually producing the

dx.doi.org/10.1021/ar500060s | Acc. Chem. Res. 2014, 47, 2332−2341

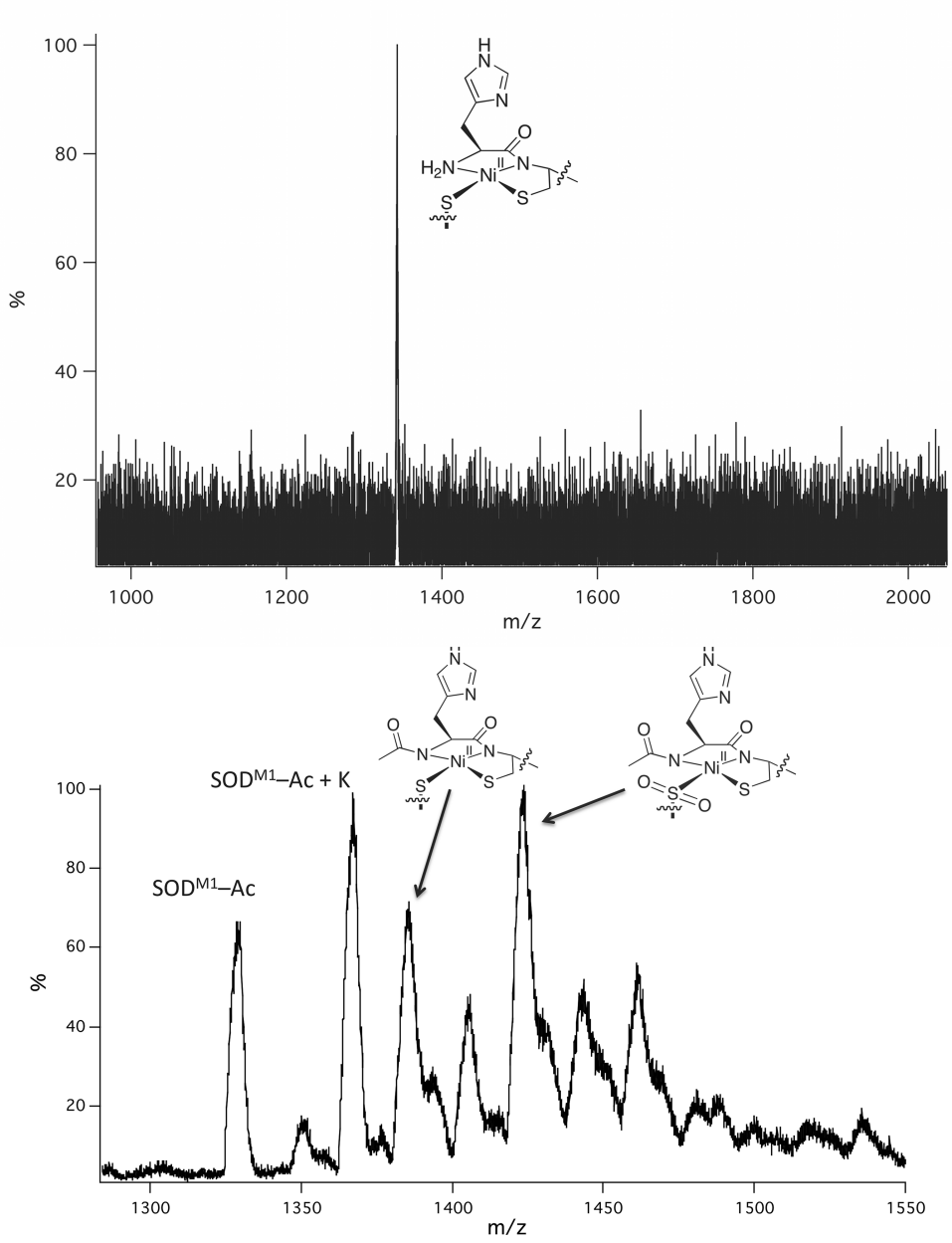

Figure 4. ESI-MS data following KO_2 addition (10 equiv) to solutions of {$Ni^{II}(SOD^{m1})$} and {$Ni^{II}(SOD^{m1}$-Ac)}. Reprinted with permission from ref 32. Copyright 2013 Elsevier.

expected trumpeting behavior (Figure 6). This is consistent with a mechanism that involves a large structural rearrangement under slow ET conditions and a small structural rearrangement under fast ET conditions. We can best rationalized this with the interconversion of a five-coordinate imidazole-ligated Ni center and a four-coordinate imidazole-dissociated species (Scheme 4). Both four- and five-coordinate Ni centers have similar ET rates (k_o ~450 s^{-1}). Imidazole ligation is rapid and thermodynamically favored upon oxidation of {$Ni^{II}(SOD^{m2})$} to {$Ni^{III}(SOD^{m2})$} (K_{on} = 3080; k_{on} = 615 s^{-1}). This can be contrasted with disassociation of the imidazole upon reduction of {$Ni^{III}(SOD^{m2})$} to {$Ni^{II}(SOD^{m2})$}, which is slow (k_{off} = 7 s^{-1}) and not as thermodynamically favored as the ligation event (K_{off} = 15). There is also an approximately −140 mV shift in the Ni^{II}/Ni^{III} redox potential upon coordination of the histidine imidazole (790 vs 650 mV vs NHE), resulting in a better electrochemical match with superoxide. These data indicate that the imidazole likely remains ligated to the Ni center under rapid catalysis (high O_2^- loads) in both the Ni(II) and Ni(III) oxidation states (Scheme 4). This both reduces the degree of structural rearrangement about the Ni center under rapid ET and tunes the redox potential such that it is electrochemically more favorable for SOD catalysis.

To probe the finer details of SOD catalysis, {Ni(SOD^{m1}-Me)} was subjected to a detailed mechanistic study.[27] O_2^- disproportionation by {Ni(SOD^{m1}-Me)} proceeds with a large room-temperature solvent H/D kinetic isotope effect (KIE ~20 vs ~7 for the classical room-temperature limit; Figure 7). This suggests that a $H^\bullet$ (or H^+) tunneling event is occurring during catalysis, a supposition supported by an Arrhenius analysis. When one considers the enzymatic kinetics, this is quite unexpected. The rate of NiSOD-catalyzed O_2^- disproportionation displays virtually no pH dependence,[16] suggesting proton transfer is not involved in the rate-limiting step of the overall

dx.doi.org/10.1021/ar500060s | Acc. Chem. Res. 2014, 47, 2332−2341

Chart 4. {Ni^{II}(SOD^{m1})} Derivatives with N-Substituted Imidazoles

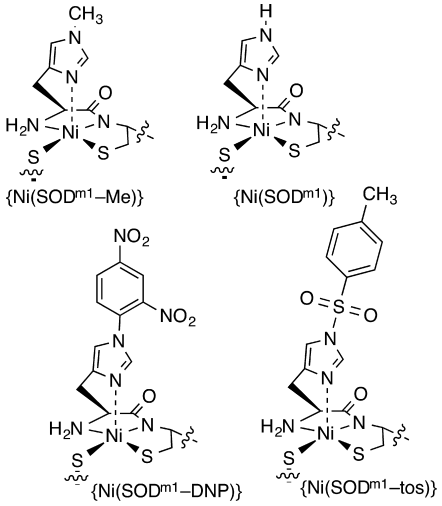

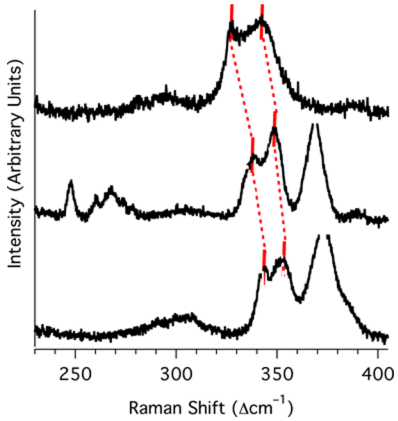

Figure 5. Resonance Raman spectra obtained from frozen solutions (77 K) of {Ni^{III}(SOD^{m1}-Me)} (top), {Ni^{II}(SOD^{m1}-DNP)} (middle), and {Ni^{III}(SOD^{m1}-Tos)} (bottom) highlighting the Ni(III)–S stretching modes.

Scheme 4. Proposed Active-Site Rearrangement of {Ni^{II}(SOD^{m2})} under Fast vs Slow Catalysis (i.e., Low vs High Superoxide Concentrations)

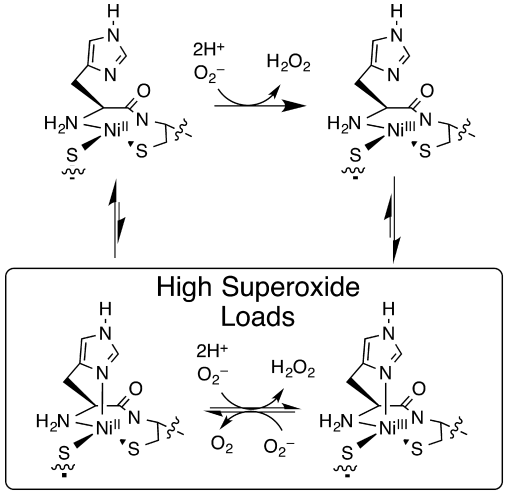

enzymatic disproportionation mechanism. Thus, fundamental mechanistic differences between the metallopeptide-based mimics of NiSOD and NiSOD itself may exist.

Considering superoxide reduction involves the transfer of both an electron and a proton and proceeds with a large solvent H/D KIE for {Ni(SOD^{m1}-Me)}-catalyzed O_2^- disproportionation, we sought to determine if {Ni^{II}(SOD^{m1}-Me)(**H**)} (protonated {Ni^{II}(SOD^{m1}-Me)}) is thermodynamically poised to participate in a proton-coupled electron-transfer-like (PCET) reaction. Addition of {Ni^{III}(SOD^{m1}-Me)} to the hydrogen atom donors TEMPO-H (O–H BDFE = 71.0 kcal mol^{-1}; BDFE: bond dissociation free energy)[49] or ascorbate (O–H BDFE = 73.6 kcal mol^{-1})[49] yielded {Ni^{II}(SOD^{m1}-Me)(**H**)} and the corresponding oxidized organic products. In contrast, 1,4 dihydroquinone (O–H BDFE = 81.5 kcal mol^{-1})[49] and hydrazine (N–H BDFE = 83.4 kcal mol^{-1})[49] would not reduce {Ni^{III}(SOD^{m1}-Me)}. This places the BDFE of the abstractable {Ni^{II}(SOD^{m1}-Me)(**H**)} hydrogen atom (i.e., the proton and electron being transferred) at less than 80 kcal mol^{-1}.

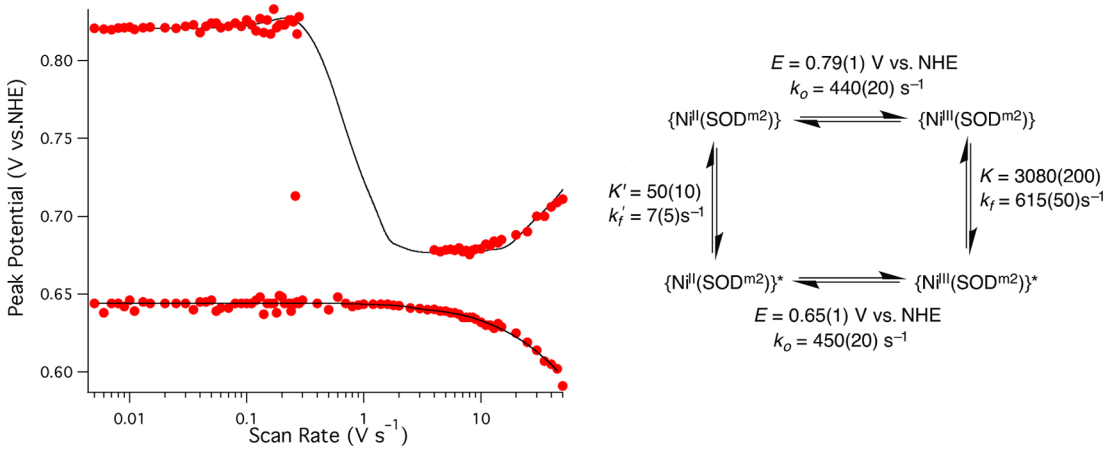

Figure 6. Thin-film cyclic voltammetry studies of {Ni(SOD^{m2})} displaying the peak position as a function of scan rate (circles). In the region between 0.5 and 3 V/s for the reduction peak positions, the reduction wave could not be deconvolved from the background capacitance. The chemical scheme depicts the simulation parameters used to fit the data (solid lines).

dx.doi.org/10.1021/ar500060s | Acc. Chem. Res. 2014, 47, 2332–2341

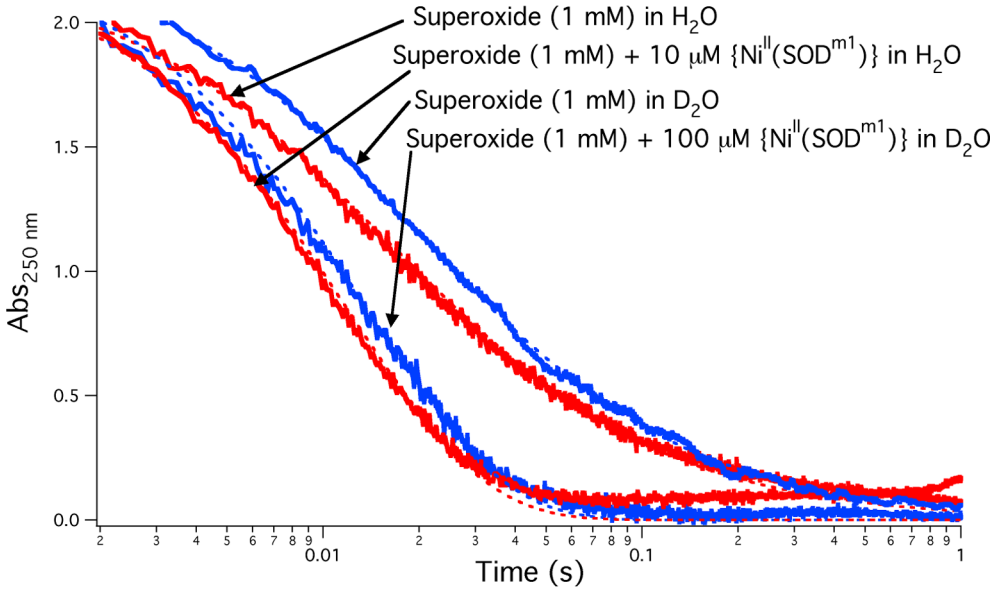

Figure 7. Stopped-flow traces for KO_2 decomposition in H_2O (red) vs D_2O (blue) in the presences vs absence of {Ni(SOD^{m1}–Me)} (pH 8.0, 20 °C).

To quantify the {Ni^{II}(SOD^{m1}-Me)(**H**)} BDFE, an equilibrium was established between TEMPO•/{Ni^{II}(SOD^{m1}-Me)(**H**)} and TEMPO-H/{Ni^{III}(SOD^{m1}-Me)}. From the $\Delta\Delta G$ of the reaction, a BDFE for {Ni^{II}(SOD^{m1}-Me)(**H**)} of 75 kcal mol^{-1} was estimated. This was reinforced by the application of a thermodynamic square scheme (Scheme 5) coupled with a

Scheme 5. Square Scheme Used To Calculate the {Ni^{II}(SOD^{m1})-Me(H)} BDFE

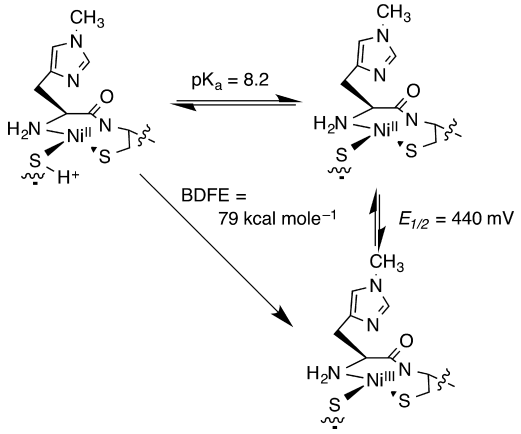

modified Bordwell equation, which yielded a {Ni^{II}(SOD^{m1}-Me)(**H**)} BDFE = 79 kcal mol^{-1}. We note that HO_2^- has a H-OO$^-$ BDFE of 81.6 kcal mol^{-1}. Thus, {Ni^{II}(SOD^{m1}-Me)(H)} is thermodynamically poised to reduce O_2^- via a PCET-like process.

Both Ni and S K-edge XAS demonstrated that the abstractable H atom within {Ni^{II}(SOD^{m1}-Me)(**H**)} is derived from a protonated Ni^{II}–S^{Cys} moiety (Ni^{II}–S(H^+)–Cys). The average Ni–S bond length decreases at low (7.5) versus high (9.5) pH, which is indicative of a Ni^{II}–S^{Cys} protonation at low pH because of alleviation of repulsive filled/filled S(3pπ)/Ni(3dπ) interactions upon protonation.[9] The S K-edge X-ray absorption spectrum of {Ni^{II}(SOD^{m1}-Me)(**H**)} also indicates a Ni^{II}–S(H^+)–Cys moiety at low pH (Figure 8). At low pH

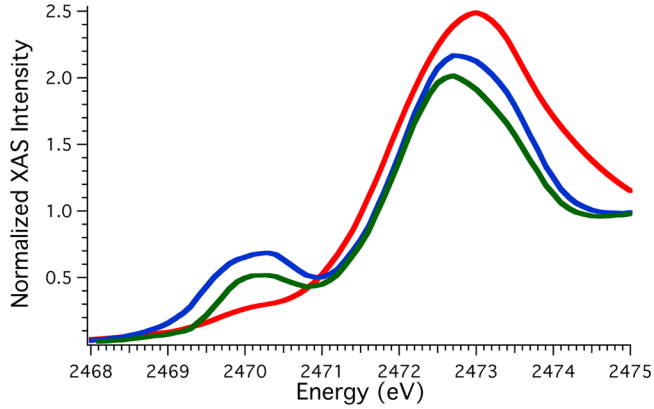

Figure 8. Sulfur K-edge spectra of {Ni^{III}(SOD^{m1}-Me)} (blue, pH 7.5), {Ni^{II}(SOD^{m1}-Me)} (red, pH 7.5), and {Ni^{II}(SOD^{m1}-Me)} (green, pH 9.5).

(7.5), there is virtually no pre-edge peak in the S K-edge spectrum and a corresponding broadening of the edge, which are indicative of the presence of a Ni^{II}–S(H^+)–Cys moiety. At high pH, the S K-edge spectrum of {Ni^{II}(SOD^{m1}-Me)} displays the predicted S(1s) → HOMO transition in the pre-edge region and a narrowing of the edge, indicating cysteinate deprotonation at high pH. No cysteinate protonation is noted at any pH for the oxidized Ni(III) form of the metallopeptide. We note that this Ni^{II}–S(H^+)–Cys moiety may provide additional protection of the cysteinate against oxidative damage. Studies probing thioether versus thiolate coordination have shown that when a S^{2-}-based lone pair is tied up in a σ bond the S atom is less susceptible to oxidative damage.[9] These data also suggest a mechanism involving the reduction of superoxide via a PCET-like reaction with the Ni^{II}–S(H^+)–Cys moiety as the "$H^{\bullet}$" source (Scheme 6). Although such a mechanism (PCET reactions originating from M^{red}–S(H^+)–R moieties) is not well documented in the literature, it may be applicable to systems other than {Ni(SOD^{m1}-Me)}, such as hydrogenases.[50]

dx.doi.org/10.1021/ar500060s | Acc. Chem. Res. 2014, 47, 2332–2341

Scheme 6. Proposed Superoxide Reduction Mechanism of {Ni^{II}(SOD^{m1})-Me(H)} and Proposed Cysteinate Protonation Site

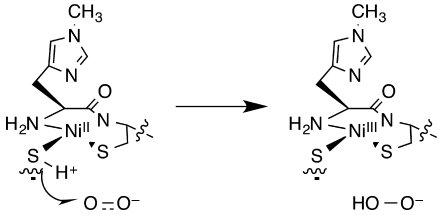

SUMMARY AND CAUTIONARY REMARKS

Over the past several years, we have shown that small metallopeptide-based NiSOD mimics can reproduce many of the structural and functional properties of NiSOD. These mimics have provided insight into (a) the necessary structural properties for efficient SOD catalysis, (b) the structural/electronic basis for Ni−S stability toward oxidizing catalytic conditions, and (c) the structural rearrangement occurring during catalysis. We also proposed a possible mechanism for NiSOD catalysis that involves a PCET-like reaction in the reduction step.

The above mimics are metallopeptides based on the NiSOD sequence itself. They may therefore seem to be more biologically relevant than "traditional" small molecule metalloprotein mimics. It cannot be overstated that this is an illusion: these maquettes remain highly minimized mimics of the biological system. They therefore lack many of the features found in NiSOD that may be vital for its structure and function. As with any metalloprotein mimic, careful comparisons between the mimic and the metalloenzyme must be made to assess the biological relevance of the biomimetic findings. In fact, mechanistic studies are already hinting at differences between the two systems. Future work on the biological system will reveal how relevant the above results are to NiSOD itself.

ASSOCIATED CONTENT

Supporting Information

Tables of selected physical parameters for Ni^{II}SOD (*S. coelicolor*) and the metallopeptides discussed in this Account. This material is available free of charge via the Internet at http://pubs.acs.org.

AUTHOR INFORMATION

Corresponding Author

*E-mail: shearer@unr.edu.

Notes

The author declares no competing financial interest.

Biography

Jason Shearer (b. 1976) received his B.S. from the University of Maryland, College Park in 1998. After completion of his Ph.D. in 2001 under Professor Julie Kovacs at the University of Washington, he performed postdoctoral work with Professor Kenneth Karilin at Johns Hopkins University from 2002−2004. He has been at the University of Nevada, Reno since 2004. His main research interests involve understanding the properties of the metal−thiolate bond and the chemistry of transition-metal/amyloidogenic protein interactions.

REFERENCES

(1) Valentine, J. S.; Wertz, D. L.; Lyons, T. J.; Liou, L. L.; Goto, J. J.; Garalla, E. B. The Dark Side of Dioxyegn Biochemistry. *Curr. Opin. Chem. Biol.* **1998**, *2*, 253−262.
(2) Imlay, J. A. How Oxygen Damages Microbes: Oxygen Tolerance and Obligate Anaerobiosis. *Adv. Microb. Physiol.* **2002**, *46*, 111−153.
(3) Beckman, J. S.; Koppenol, W. H. Nitric Oxide, Superoxide, and Peroxynitrite: The Good, The Bad, and Ugly. *Am. J. Physiol.: Cell Physiol.* **1996**, *271*, C1424−C1437.
(4) Sawyer, D. T.; Valentine, J. S. How Super Is Superoxide? *Acc. Chem. Res.* **1981**, *14*, 393−400.
(5) Miller, A.-F. Superoxide Dismutase: Active Sites That Save, but a Protein that Kills. *Curr. Opin. Chem. Biol.* **2004**, *8*, 162−168.
(6) Broering, E. P.; Truong, P. T.; Gale, E. M.; Harrop, T. C. Synthetic Analogues of Nickel Superoxide Dismutase: A New Role for Nickel in Biology. *Biochemistry* **2013**, *52*, 4−18.
(7) Bryngelson, P. A.; Maroney, M. J. Nickel Superoxide Dismutase. In *Metal Ions in Life Sciences*; Sigel, A., Sigel; H., Sigel, R. K. O., Eds.; John Wiley & Sons, Ltd.: Chichester, England, 2007; Vol. *2*, pp 417−444.
(8) Fridovich, I. Superoxide Dismutase. In *Encyclopedia of Biological Chemistry*, 1st ed.; Lennarz, W. J., Lane, M. D., Eds.; Elsevier: Oxford, 2004; Vol. *4*, pp 135− 138.
(9) Grapperhaus, C. A.; Darensbourg, M. Y. Oxygen Capture by Sulfur in Nickel Thiolates. *Acc. Chem. Res.* **1998**, *31*, 451−459.
(10) Lee, J. W.; Roe, J. H.; Kang, S. O. Nickel-Containing Superoxide Dismutase. *Methods Enzymol.* **2002**, *349*, 90−101.
(11) Youn, H.-D.; Kim, E.-J.; Roe, J.-H.; Hah, Y.-C.; Kang, S.-O. A Novel Nickel-Containing Superoxide Dismutase from *Streptomyces* spp. *Biochem. J.* **1996**, *318*, 889−896.
(12) Youn, H.-D.; Youn, H.; Lee, J.-W.; Hah, Y.-C.; Kang, S.-O. Unique Isozymes of Superoxide Dismutase in *Streptomyces griscus*. *Arch. Biochem. Biophys.* **1996**, *334*, 341−348.
(13) Palenik, B.; Brahamsha, B.; Larimer, F. W.; Land, M.; Hauser, L.; Cuhain, P.; Lamerdin, J.; Regala, W.; Allen, E. E.; McCarren, J.; Paulsen, I.; Dufresne, A.; Partensky, F.; Webb, E. A.; Waterbury, J. The Genome of Motile Marine *Synechococcus*. *Nature* **2003**, *424*, 1037−1042.
(14) DuPont, C. L.; Neupane, K.; Shearer, J.; Palenik, B. Diversity, Function and Evolution of Genes Coding for Putative Ni-Containing Superoxide Dismutase. *Environ. Microbiol.* **2008**, *10*, 1831−1843.
(15) Choudhury, S. B.; Lee, J.-W.; Davidson, G.; Yim, Y.-I.; Bose, K.; Sharma, M. L.; Kang, S.-O.; Cabelli, D. E.; Maroney, M. J. Examination of the Nickel Site Structure and Reaction Mechanism in *Streptomyces seoulensis* Superoxide Dismutase. *Biochemistry* **1999**, *38*, 3744−3752.
(16) Bryngelson, P. A.; Arobo, S. E.; Pinkham, J. L.; Cabelli, D. E.; Maroney, M. J. Expression, Reconstitution, and Mutation of Recombinant *Streptomyces coelicolor* NiSOD. *J. Am. Chem. Soc.* **2004**, *126*, 460−461.
(17) Szilagyi, R. K.; Bryngelson, P. A.; Maroney, M. J.; Hedman, B.; Hodgson, K. O.; Solomon, E. I. S K-edge X-ray Absorption Spectroscopic Investigation of the Ni-Containing Superoxide Dismutase Active Site: New Structural Insight into the Mechanism. *J. Am. Chem. Soc.* **2004**, *126*, 3018−3019.
(18) Wuerges, J.; Lee, J.-W.; Yim, Y.-I.; Yim, H.-S.; Kang, S.-O.; Carugo, K. D. Crystal Structure of Nickel Containing Superoxide Dismutase Reveals another Type of Active Site. *Proc. Natl. Acad. Sci. U.S.A.* **2004**, *101*, 8569−8574.
(19) Barondeau, D. P.; Kassmann, C. J.; Bruns, C. K.; Tainer, J. A.; Getzoff, E. D. Nickel Superoxide Dismutase Structure and Mechanism. *Biochemistry* **2004**, *43*, 8038−8047.
(20) Herbst, R. W.; Guce, A.; Bryngelson, P. A.; Higgins, K. A.; Ryan, K. C.; Cabelli, D. E.; Garman, S. C.; Maroney, M. J. Role of Conserved Tyrosine Residues in NiSOD Catalysis: A Case of Convergent Evolution. *Biochemistry* **2009**, *48*, 3354−3369.
(21) Pelmenschikov, V.; Siegbahn, P. E. M. Nickel Superoxide Dismutase Reaction Mechanism Studied by Hybrid Density Functional Methods. *J. Am. Chem. Soc.* **2006**, *128*, 7466−7475.

(22) Fiedler, A. T.; Bryngelson, P. A.; Maroney, M. J.; Brunold, T. C. Spectroscopic and Computational Studies of Ni Superoxide Dismutase: Electronic Structure Contributions to Enzymatic Function. *J. Am. Chem. Soc.* **2005**, *127*, 5449−5462.
(23) Kovacs, J. A. Cysteinate-Ligated Non-Heme Iron and Non-Corrinoid Cobalt Enzymes. *Chem. Rev.* **2004**, *104*, 825−848.
(24) Wu, M.; Beckham, G. T.; Larsson, A. M.; Ishida, T.; Kim, S.; Payne, C. M.; Himmel, M. E.; Crowley, M. F.; Horn, S. J.; Westerneg, B.; Igarashi, K.; Samejima, M.; Stahlberg, J.; Eijsink, V. G. H.; Sandgren, M. Crystal Structure and Computational Characterization of the Lytic Polysaccharide Monooxygenase GH61D from Basidiomycota Fungus *Phanerochaete chrysosporium*. *J. Biol. Chem.* **2013**, *288*, 12828−12839.
(25) Komori, H.; Inagaki, S.; Yosioka, S.; Aono, S.; Higuchi, Y. Crystal Structure of CO-Sensing Transcription Activator CooA Bound to Exogenous Ligand Imidazole. *J. Mol. Biol.* **2007**, *367*, 864−871.
(26) Ragsdale, S. W. Nickel-Based Enzyme Systems. *J. Biol. Chem.* **2009**, *284*, 18571−18575.
(27) Shearer, J. Use of a Metallopeptide-Based Mimic Provides Evidence for a Proton-Coupled Electron-Transfer Mechanism for Superoxide Reduction by Nickel-Containing Superoxide Dismutase. *Angew. Chem., Int. Ed.* **2013**, *52*, 2569−2572.
(28) Shearer, J.; Long, L. M. A Nickel Superoxide Dismutase Maquette That Reproduces the Spectroscopic and Functional Properties of the Metalloenzymes. *Inorg. Chem.* **2006**, *45*, 2358−2360.
(29) Neupane, K. P.; Shearer, J. The Influence of Amine/Aimide vs. Bisamide Coordination in Nickel Superoxide Dismutase. *Inorg. Chem.* **2006**, *45*, 10552−10566.
(30) Neupane, K. P.; Gearty, K.; Francis, A.; Shearer, J. Probing Variable Axial Ligation in Nickel Superoxide Dismutase Utilizing Metallopeptide-Based Models: Insight into the Superoxide Disproportionation Mechanism. *J. Am. Chem. Soc.* **2007**, *129*, 14605−14618.
(31) Shearer, J.; Neupane, K. P.; Callan, P. E. Metallopeptide Based Mimics with Substituted Histidines Approximate a Key Hydrogen Bonding Network in the Metalloenzyme Nickel Superoxide Dismutase. *Inorg. Chem.* **2009**, *48*, 10560−10571.
(32) Shearer, J. Dioxygen and Superoxide Stability of Metallopeptide Based Mimics of Nickel Containing Superoxide Dismutase: The Influence of Amine/Amidate vs. Bis-Amidate Ligation. *J. Inorg. Biochem.* **2013**, *129*, 145−149.
(33) Shearer, J.; Zhao, N. $[Me_4N](Ni^{II}(BEAAM))$: A Synthetic Model for Nickel Superoxide Dismutase That Contains Ni in a Mixed Amine/Amide Coordination Environment. *Inorg. Chem.* **2013**, *45*, 9637−9639.
(34) Shearer, J.; Dehestani, A.; Abanda, F. Probing Variable Amine/Amide Ligation in $Ni^{II}N_2S_2$ Complexes Using Sulfur K-Edge and Nickel L-Edge X-ray Absorption Spectroscopies: Implication for the Active Site of Nickel Superoxide Dismutase. *Inorg. Chem.* **2008**, *47*, 2649−2660.
(35) Mathrubootham, V. T.; Staples, J.; McCraken, R.; Shearer, J.; Hegg, J.; Bisamidate, E. L. Mixed Amine/Amidate NiN_2S_2 Complexes as Models for Nickel-Containing Acetyl Conenzyme A Synthase and Superoxide Dismutase: An Experimental and Computational Study. *Inorg. Chem.* **2010**, *49*, 5393−5406.
(36) Robertson, D. E.; Farid, R. S.; Moser, C. C.; Urbauer, J. L.; Mulholland, S. E.; Pidikiti, R.; Lear, J. D.; Wand, A. J.; DeGrado, W. F.; Dutton, P. L. Design and Synthesis of Multi-Haem Proteins. *Nature* **1994**, *368*, 425−432.
(37) Reedy, C. J.; Gibney, B. R. Heme Protein Assemblies. *Chem. Rev.* **2004**, *104*, 617−649.
(38) Schmidt, M.; Zahn, S.; Carella, M.; Ohlenschlager, O.; Gorlach, M.; Kothe, E.; Weston, J. Solution Structure of a Functional Biomimetic and Mechanistic Implications for Nickel Superoxide Dismutase. *ChemBioChem.* **2008**, *9*, 2135−2146.
(39) Tietze, D.; Breitzke, H.; Imhof, D.; Kothe, E.; Weston, J.; Buntkowsky, G. New Insight into the Mode of Action of Nickel Superoxide Dismutase Investigating Metallopeptide Substrate Models. *Chem.—Eur. J.* **2004**, *15*, 5517−523.
(40) Mead, B. G. Synthesis and Characterization of a Model Nickel Superoxide Dismutase Metallopeptide Functionalized for Hydrogen Production. M.S. Thesis, University of Nevada, Reno, Reno, NV, January 2014.
(41) Grapperhaus, C. A.; Mullins, C. S.; Kozlowski, P. M.; Mashuta, M. S. Synthesis and Oxygenation of a Nickel(II) and Zinc(II) Dithiolate: An Experimental and Theoretical Comparison. *Inorg. Chem.* **2004**, *43*, 2859−2866.
(42) Kruger, H. J.; Peng, G.; Holm, R. H. Low-Potential Nickel(III,II) Complexes: New Systems Based on Tetradentate Amidate-Thiolate Ligands and the Influence of Ligand Structure on Potentials in Relation to the Nickel Site in [NiFe]-Hydrogenase. *Inorg. Chem.* **1991**, *30*, 734−742.
(43) Mullins, C. S.; Grapperhaus, C. A.; Kozlowski, P. M. Density Functional Theory Investigations of NiN_2S_2 Reactivity as a Function of Nitrogen Donor Type and N-H···S Hydrogen Bonding Inspired by Nickel-Containing Superoxide Dismutase. *J. Biol. Inorg. Chem.* **2006**, *11*, 617−625.
(44) Herdt, D. R.; Grapperhaus, C. A. Kinetic Study of Nickel-Thiolate Oxygenation by Hydrogen Peroxide. Implications for Nickel-Containing Superoxide Dismutase. *Dalton Trans.* **2012**, *41*, 364−366.
(45) Green, K. N.; Brothers, S. M.; Jenkins, R. M.; Carson, C. E.; Grapperhaus, C. A.; Darensbourg, M. Y. An Experimental and Computational Study of Sulfur-Modified Nucleophilicity in a Dianionic NiN_2S_2 Complex. *Inorg. Chem.* **2007**, *46*, 7536−7544.
(46) Gale, E. M.; Narendrapurapu, B. S.; Simmonett, A. C.; Schaefer, H. F.; Harrop, T. C. Exploring the Effects of H-Bonding in Synthetic Analogues of Nickel Superoxide Dismutase (Ni-SOD): Experimental and Theoretical Implications for Protection of the Ni-SCys Bond. *Inorg. Chem.* **2010**, *49*, 7080−7096.
(47) Solomon, E. I.; Szilagyi, R. K.; DeBeer George, S.; Basumallick, L. Electronic Structures of Metal Sites in Proteins and Models: Contributions to Function in Blue Copper Proteins. *Chem. Rev.* **2004**, *104*, 419−458.
(48) Hirst, J.; Armstrong, F. A. Fast-Scan Cyclic Voltammetry of Protein Films of Pyrolytic Graphite Edge Electrodes: Characteristics of Electron Exchange. *Anal. Chem.* **1998**, *70*, 5062−5071.
(49) Warren, J. J.; Tronic, T. A.; Mayer, J. M. Thermochemistry of Proton-Coupled Electron-Transfer Reagents and Its Implications. *Chem. Rev.* **2010**, *110*, 6961−7001.
(50) Lubitz, W.; Ogata, H.; Rüdiger, O.; Reijerse, E. Hydrogenases. *Chem. Rev.* **2014**, *114*, 4081−4148.